

# Lidar detection of high concentrations of ozone and aerosol transported from Northeast Asia over Saga, Japan

Osamu Uchino<sup>1, 2</sup>, Tetsu Sakai<sup>2</sup>, Toshiharu Izumi<sup>2</sup>, Tomohiro Nagai<sup>2</sup>, Isamu Morino<sup>1</sup>, Akihiro Yamazaki<sup>2</sup>, Makoto Deushi<sup>3</sup>, Keiya Yumimoto<sup>2</sup>, Takashi Maki<sup>2</sup>, Taichu Y. Tanaka<sup>2</sup>, Taiga Akaho<sup>4</sup>, Hiroshi Okumura<sup>4</sup>, Kohei Arai<sup>4</sup>, Takahiro Nakatsuru<sup>1</sup>, Tsuneo Matsunaga<sup>1</sup>, Tatsuya Yokota<sup>1</sup>

<sup>1</sup>National Institute for Environmental Studies, 16-2 Onogawa, Tsukuba, Ibaraki 305-8506, Japan

<sup>2</sup>Meteorological Research Institute, 1-1 Nagamine, Tsukuba, Ibaraki 305-0052, Japan

<sup>3</sup>Japan Meteorological Agency, 1-3-4 Otemachi, Chiyoda-ku, Tokyo 100-8122, Japan

<sup>4</sup>Saga University, 1 Honjou, Saga, Saga 840-8502, Japan

*Correspondence to:* O. Uchino (uchino.osamu@nies.go.jp)

**Abstract.** To validate products of the Greenhouse gases Observing SATellite (GOSAT), we observed vertical profiles of aerosols, thin cirrus clouds, and tropospheric ozone with a mobile lidar system that consisted of a two-wavelength (532 and 1064 nm) polarization lidar and a tropospheric ozone Differential Absorption Lidar (DIAL). We used these lidars to make continuous measurements over Saga (33.24°N, 130.29°E) during 20–31 March 2015. High ozone and high aerosol concentrations were observed almost simultaneously in the altitude range 0.5–1.5 km from 03:00 to 20:00 Japan Standard Time on 22 March 2015. The maximum ozone volume mixing ratio was ~110 ppbv. The maxima of the aerosol extinction coefficient and optical depth at 532 nm were 1.2 km<sup>-1</sup> and 2.1, respectively. Backward trajectory analysis and the simulations by the Model of Aerosol Species IN the Global Atmosphere (MASINGAR) mk-2 and the Meteorological Research Institute Chemistry-Climate Model, version 2 (MRI-CCM2) indicated that mineral dust particles originated from the Gobi Desert and an air mass with high ozone and aerosol (mainly sulfate) concentrations originated from the North China Plain could have been transported over the measurement site within about two days. These high ozone and aerosol concentrations impacted surface air quality substantially in the afternoon of 22 March 2015. After some modifications of its physical and chemical parameters, MRI-CCM2 approximately reproduced the high-ozone volume-mixing ratio. The MASINGAR mk-2 successfully predicted high aerosol concentrations, but the predicted peak aerosol optical thickness was about one-third of the observed value.

## 1 Introduction

Tropospheric ozone is a major air pollutant and impacts human health and vegetation (HTAP, 2010; Yue and Unger, 2014). It is also an important greenhouse gas (IPCC, 2013). Tropospheric aerosols are also air pollutants and aggravate respiratory conditions (HTAP, 2010). Tropospheric aerosols also enhance radiative forcing in a negative (sulfuric acid particles) or positive (black carbon) way (IPCC, 2013), and they affect remote sensing such as the measurement of greenhouse gases from space (Houweling et al., 2005; Uchino et al., 2012a). It is therefore very important to monitor tropospheric ozone and aerosols and to understand their temporal and spatial variations. The aerosols transported from the East Asia to the western Japan were observed by lidar and their vertical distributions were reported (Iwasaka et al., 1988; Murayama et al., 2001; Hara et al., 2009). On the other hand the ozone pollutions from the Asia were mainly studied by the surface measurements (Akimoto et al., 1996; Yamaji et al., 2006). Continuous ozone vertical distributions by ozone DIAL are very useful for studying the transport process and the origin.

To validate products of the Greenhouse gases Observing SATellite (GOSAT), we developed a two-wavelength (532 and 1064 nm) polarization lidar (hereafter abbreviated as Mie lidar) to observe vertical profiles of tropospheric and stratospheric aerosols and thin cirrus clouds at the National Institute for Environmental Studies (NIES), Tsukuba (36.05°N, 140.13°E), Japan in 2009. In 2010 we also developed a Differential Absorption Lidar (DIAL) to measure tropospheric ozone profiles (hereafter abbreviated as ozone DIAL). The ozone DIAL was installed in a container with the Mie lidar. In March 2011, we moved the lidar container to Saga (33.24°N, 130.29°E) in the Kyushu district of western Japan at a location 2.6 m above sea level. The ozone DIAL was modified in September 2012 (Uchino et al., 2014).

Mie lidar has been used to demonstrate the influence of high-altitude aerosols and cirrus clouds on the GOSAT product of the column-averaged dry air mole fraction of carbon dioxide ( $XCO_2$ ) retrieved from the Thermal And Near infrared Sensor for carbon Observation-Fourier Transform Spectrometer (TANSO-FTS) Short-Wavelength InfraRed (SWIR) spectral data onboard GOSAT. The  $XCO_2$  data were improved by taking the vertical profiles of aerosols and cirrus clouds measured by Mie lidar into account (Uchino et al., 2012a). The increases of stratospheric aerosols caused by the 2009 Sarychev eruption and the 2011 Nabro eruption were observed by Mie lidar (Uchino et al., 2012b).

Ozone DIAL has been used to validate the GOSAT ozone product retrieved from TANSO-FTS Thermal InfraRed (TIR) spectral data (Ohya et al., 2012), to observe ozone concentrations in the lower troposphere, and to compare the observed concentrations with those predicted by the Meteorological Research Institute Chemistry-Climate Model, version 2 (MRI-CCM2) (Deushi and Shibata, 2011). Use of Mie lidar and ozone DIAL will facilitate satellite product validation not only for GOSAT but also for upcoming satellites such as the TROPOspheric Monitoring Instrument (TROPOMI, Veefkind et al., 2012) and the Geostationary Environment Monitoring Spectroscopy (GEMS, Bak et al., 2013). High ozone episodes in the lower troposphere have been observed by lidar (Banta et al., 1998; Koutidis et al., 2002; Ancellet et al., 2005; Eisele and Trickl, 2005; Kuang et al., 2011). These observation records were limited

to one week at most. We made an 11-day continuous record on 20–31 March 2015.

In this paper we report an event during which high concentrations of ozone and aerosols were observed almost simultaneously below an altitude of 1.5 km over Saga on 22 March 2015 by Mie lidar and ozone DIAL, which substantially impacted surface air quality. We also compared the observational results with those simulated by the models.

## 2 Characteristics of lidar system and observation parameters

Mie lidar and ozone DIAL were installed in a container with dimensions of about 228 cm (width), 683 cm (length), and 255 cm (height), as shown in Fig. 1. Mie lidar is a two-wavelength (532 and 1064 nm) polarization lidar based on a neodymium-doped yttrium-aluminum-garnet (Nd:YAG) laser; the characteristics are summarized in Table 1. The output energy at 532 and 1064 nm was 130 mJ, with a pulse repetition rate of 10 Hz. The diameter of the receiving telescope was 30.5 cm. The output signals from the photomultiplier tubes (PMT) and a silicon avalanche photodiode (APD) were processed by transient recorders with a 12-bit analog/digital converter and a photon counter.

The data analysis methods of Mie lidar and ozone DIAL have been described by Uchino et al. (2012b) and Uchino et al. (2014), respectively. We summarize the observation parameters obtained by Mie lidar. The backscattering ratio  $R$  is defined as

$$R = (BR + BA)/BR, \quad (1)$$

where  $BR$  and  $BA$  are the Rayleigh and Mie backscattering coefficients, respectively. Backscattering ratio profiles were derived by the inversion method (Fernald, 1984). The reference altitude was usually set between 9 and 12 km where only molecular backscattering could be assumed when there were no clouds. We assumed the lidar ratio  $LR$  (extinction-to-backscatter ratio) for aerosols to be 50 sr at 532 nm and 45 sr at 1064 nm based on the lidar ratios for Asian dust and pollution aerosols summarized by Sakai et al. (2003), Anderson et al. (2003) and Cattrall et al. (2005). Their summaries are as follows: Sakai et al. (2003): Asian dust  $47 \pm 18$  sr, Cattrall et al. (2005): dust (spheroids)  $42 \pm 4$  sr, South East Asia pollution  $58 \pm 10$  sr, Anderson et al. (2003): ACE-Asia pollution (fine-dominated, submicron portion)  $50 \pm 5$  sr, dust (coarse-dominated, dust-like chemistry, supermicron portion)  $46 \pm 8$  sr. As a simplification, we used the same value for both species. To calculate  $BR$ , we used the atmospheric molecular density profiles obtained by operational radiosondes at the Fukuoka District Meteorological Observatory (33.58°N, 130.38°E), Japan Meteorological Agency (JMA). The aerosol extinction coefficient was calculated by multiplying  $BA$  by  $LR$ .

The total volume depolarization ratio  $D$  was defined as

$$D = S / (P + S) \cdot 100 (\%), \quad (2)$$

where  $P$  and  $S$  are the parallel and perpendicular components of the backscattered signals, respectively. The particle depolarization ratio  $D_p$  was obtained from the equation

$$D_p = (D \cdot R - D_m) / (R - 1), \quad (3)$$

where  $D_m$  is the atmospheric molecular depolarization ratio. We used a  $D_m$  value of 0.37% for this lidar system; we calculated  $D_m$  from the spectral transmission data of the interference filter at 532 nm and the Rayleigh backscattering cross sections (Sakai et al., 2003). The value of  $D_p$  indicates whether the particles are spherical or non-spherical; large values indicate the presence of non-spherical particles. The backscatter-related Ångström exponent  $Alp$ , the qualitative indicator of aerosol particle size, is defined by

$$BA(\lambda) \propto \lambda^{-Alp}, \quad (4)$$

where  $\lambda$  is the wavelength. Larger values of  $Alp$  indicate the predominance of smaller (i.e., submicrometer-sized) particles. The vertical resolution of these observation parameters was 150 m, and the time resolution was set to be 1 h for comparison with the Model of Aerosol Species in the Global Atmosphere (MASINGAR)-mk2 (Yukimoto et al., 2012). The lowest altitude of Mie lidar measurement was 225 m due to the non-perfect overlap of the transmitter-receiver optical axes of the lidar system.

The ozone DIAL consisted of a Nd:YAG laser and a 2-m-long Raman cell filled with CO<sub>2</sub> gas that generated four Stokes lines from stimulated Raman scattering by CO<sub>2</sub>; the characteristics are summarized in Table 2. In this study, we used three Stokes lines (276, 287, and 299 nm). The output energies of these Stokes lines were about 8–9 mJ per pulse, with a pulse repetition rate of 10 Hz. The receiving telescope diameters were 10 cm for boundary layer ozone measurements and 49 cm for free tropospheric ozone measurements. The Mie lidar and ozone DIAL were synchronized by two pulse-delay generators.

The 276/287 nm and 287/299 nm wavelength pairs were used for ozone DIAL measurements in the altitude ranges of 0.57–2.0 km and 2.0–6.0 km, respectively. The effective vertical resolutions were 270 m for 0.57–2.0 km and 540 m for 2.0–6.0 km, respectively (Uchino et al., 2014). The time resolution was set to 1 h to facilitate comparison with the MRI-CCM2. The aerosol correction was not made for the ozone retrieval. Next, we report the continuous lidar observational results made at Saga from 20 March to 31 March 2015.

### 3 Ozone DIAL data

Figure 2a shows a time-altitude cross-section of ozone volume mixing ratios observed by DIAL at Saga from 11:10 JST on 20 March to 14:33 JST on 31 March 2015. Lidar observations were not obtained from 15:56 JST on 27 March to 21:58 JST on 29 March 2015, mainly because of rainy or cloudy conditions.

We made quality checks of the DIAL data. The gray regions in Fig. 2a correspond to areas where there were no observational data or the errors were larger than 10%. The errors were computed from the lidar signal-to-noise ratios by use of Poisson statistics. Regions surrounded by a black rectangle are areas where the data were affected by aerosols and/or clouds with  $R$  larger than 2 at 299 nm, which were calculated assuming  $LR=50$  sr without correcting attenuation by ozone absorption. In the lowest row of Fig. 2a, we show hourly data of surface oxidant volume mixing ratios (Ox) at Takagimachi in Saga city measured by the Saga Prefectural Environmental Research Center ([https://www.pref.saga.lg.jp/web/contents/kankyo1/shisetsu/\\_40810/\\_41304/\\_67819.html](https://www.pref.saga.lg.jp/web/contents/kankyo1/shisetsu/_40810/_41304/_67819.html)). Takagimachi is located about 2.8 km northeast from the ozone DIAL site. Because the surface Ox was observed by an UV photometer, the contribution of other components such as peroxyacetyl nitrate (PAN) to oxidant concentrations was extremely low, and the oxidant volume mixing ratio was considered to be that of ozone.

Figure 2a indicates that the ozone volume mixing ratios measured by DIAL were usually about 50–70 ppbv during the study period. Comparatively high ozone concentrations, >75 ppbv, were detected at altitudes of 0.57–3 and 0.57–2 km on 20–23 March and 30–31 March, respectively. Notably high ozone volume mixing ratios of 90–110 ppbv at altitudes of 0.57–1.5 km were observed from 03:00 to 20:00 JST on 22 March. These high ozone concentrations were also seen in the surface photochemical oxidants data, i.e., the Ox equaled 92–101 ppbv from 15:00 to 21:00 JST on 22 March, as shown in the lowest row in Fig. 2a. The maximum concentration of Ox was 101 ppbv at 16:00 JST. This maximum value was far above the environmental quality standard of 60 ppbv for hourly photochemical oxidants in Japan (<https://www.env.go.jp/en/air/aq/aq.html>).

### 3.1 Comparison of DIAL data with MRI CCM-2

The MRI-CCM2 is a global model that simulates chemical and physical processes that affect the distribution and evolution of ozone and other trace gases from the surface to the stratosphere (Deushi and Shibata, 2011). Uchino et al. (2014) have provided an outline of MRI-CCM2. The vertical resolution of the model increases from about 100 to 600 m from the surface to 6 km. The time step of the transport (chemistry) scheme is 30 (15) min. We used hourly model output data. The horizontal resolution is about 110 km. We examined whether or not the model could simulate DIAL observational results. The MRI-CCM2 simulated the DIAL observations reasonably well. However, the MRI-CCM2 predicted the high ozone concentrations of 50–60 ppbv and could not reproduce those of 90–110 ppbv observed with DIAL below an altitude of 1.5 km during 03:00–20:00 JST on 22 March 2015.

We therefore performed some simulations in which we changed the emission inventory data and the term that forced the reanalysis wind field. The most reasonable results which were shown in Fig. 2b were obtained when the following changes were made. The e-folding time of the nudging term was changed from 18 hours to 12 hours to more strongly force the simulated wind fields toward the reanalysis data. In addition, we changed the emission inventory of Regional Emission inventory in Asia version 1.1 (REAS 1.1) (Ohara et al., 2007) to the REAS 2.1 emission inventory in 2007 (Kurokawa et al., 2013) and the

NO<sub>2</sub>/NO<sub>x</sub> emissions ratio from 5% to 15% by volume, which is within the range of uncertainty (Carslaw, 2005). The emission inventory of NO<sub>x</sub> increased about 50% from REAS 1.1 to REAS 2.1. Figure 2c shows the differences between the observed and simulated ozone mixing ratios. Simulated ozone volume mixing ratios were about 60–70 ppbv below an altitude of 1.5 km from 14:00 JST on 21 March to 21:00 JST on 22 March 2015, lower by about 20–50 ppbv compared with the DIAL results. And the MRI-CCM2 predicted the high ozone concentration a half day earlier than the DIAL observation.

The maximum bias (systematic error) of ozone DIAL data caused by aerosols was estimated to be 20% (15 ppbv) at 0.57 km, and the mean bias and the standard deviation were  $7\% \pm 5\%$  in the altitude range 0.57–2.0 km at 11:00 JST. These biases were estimated from *Alp* observed at the same time by Mie lidar and assuming  $LR=50$  sr in the wavelength range 276–299 nm, based on the equations of (6) and (7) in Uchino and Tabata (1991). These biases were not large since the 276/287 nm and 287/299 nm wavelength pairs were suitable for measurements of ozone in the boundary layer and the free troposphere respectively (Nakazato et al., 2007). As mentioned earlier, the ozone DIAL data with the statistical error smaller than 10% was used in this study. Therefore the uncertainty of the ozone DIAL data was estimated to be smaller than 22% and the mean value of the uncertainty was 12%. A model with higher horizontal resolution might be necessary to more realistically simulate high surface ozone concentration events in the planetary boundary layer.

#### 4 Mie lidar data

Figures 3a, 3b, and 3c show time-altitude cross-sections of the backscattering ratio ( $R$ ), the total volume depolarization ratio ( $D$ ), and the particle depolarization ratio ( $D_p$ ), respectively, observed by Mie lidar at Saga from 11:10 JST on 20 March to 14:33 JST on 31 March 2015. Mie lidar data were not obtained from 15:56 JST on 27 March to 21:58 JST on 29 March 2015, mainly because of rainy or cloudy conditions. We made quality checks of Mie lidar data. Gray regions are areas where there were no observational data or the data were affected by clouds.

Aerosol layers with  $R$  in the range 2–4 almost always existed below an altitude of 2.5 km for 20–31 March 2015. An event of high aerosol loading with large values of  $R$  ( $>8$ ) was observed below altitudes of 1.5 km for 03:00–21:00 JST on 22 March, when the values of  $D$  were small (the mean and the standard deviation:  $3.9 \pm 2.1\%$ ) compared with those before and after the event, when the values of  $D$  were larger than  $7.9 \pm 2.1\%$  during 15:00 JST on 21 through 15:00 JST on 23, except for 03:00–21:00 JST on 22. The main aerosol component during the event might be submicrometer-sized spherical particles, because  $D_p$  was small ( $4 \pm 2\%$ ), and the wavelength exponent *Alp* was large ( $1.3 \pm 0.3$ ). In contrast, the main aerosol particles before and after the event could be supermicrometer-sized, nonspherical mineral dust particles because  $D_p$  was comparatively large ( $13 \pm 3\%$ ) and *Alp* was  $1.0 \pm 0.2$  (Sakai et al., 2003; Catrall et al., 2005). When there were no clouds above,  $R$  at 1064 nm was estimated assuming *Alp*=1.5 at the reference altitude where very small amount of aerosols was expected to be present, i.e.,  $R=1.06 \pm 0.06$

( $D=1.2 \pm 0.5$ ) at 532 nm, in the altitude range 3–6 km. If the value of  $Alp$  was changed from 1.0 to 2.0 at the reference altitude, the uncertainty in  $Alp$  was estimated to be  $\pm 0.2$ .  $Alp$  was 0.3–2.0 in the 11-day Mie lidar record. The maximum errors of  $D$  and  $D_p$  were 0.1% and 2% for  $R>2$  at 532 nm.

During the same time period, high aerosol concentrations were also observed at the surface (Fig.4). Hourly values of the mass concentrations of particulate matter with a diameter of 2.5  $\mu\text{m}$  or less ( $\text{PM}_{2.5}$ ) at Takagimachi measured by the Saga Prefectural Environmental Research Center were 23  $\mu\text{g m}^{-3}$  at 10:00 JST and increased up to a maximum value of 110  $\mu\text{g m}^{-3}$  at 15:00 JST on 22 March; the concentrations were greater than 82  $\mu\text{g m}^{-3}$  during 13:00–16:00 JST and decreased to 17  $\mu\text{g m}^{-3}$  at 01:00 JST on 23 March. The daily mean value of  $\text{PM}_{2.5}$  was 50.6  $\mu\text{g m}^{-3}$  for 24 hours on 22 March at Takagimachi, larger than the environmental quality standard of 35  $\mu\text{g m}^{-3}$  in Japan (<https://www.env.go.jp/en/air/aq/aq.html>).

#### 4.1 Comparison of Mie lidar data with MASINGAR mk-2

The MASINGAR-mk2 is an improved version of the MASINGAR aerosol model (Tanaka et al., 2003); it treats five aerosol species: sulfate, black and organic carbon, sea salt, and soil dust. We used emission data for sulfur dioxide and for black and organic carbon from MACCity (Granier et al., 2011). Soil dust and sea salt were represented by 10 bins with particle diameters of 0.2–20  $\mu\text{m}$ . The model was coupled online with the atmospheric general circulation model MRI-AGCM3 (Yukimoto et al., 2012). The Meteorological fields were from JMA Global Analysis data (GANAL). The horizontal resolution of the MASINGAR-mk2 was about 60 km, and the number of vertical layers was 40 from the surface to 0.1 hPa. The vertical resolutions were 100, 300, and 600 m at the lowest level and altitudes of 1 and 6 km, respectively. The time step of the transport (chemistry) scheme was 450 seconds, and we used hourly model output data.

Figures 4a and 4b show the time-height cross sections of aerosol extinction coefficients observed by Mie lidar and simulated by MASINGAR-mk2, respectively. Figure 4c represents the difference between the observed and simulated extinction coefficients. The model was able to capture the general characteristics of the observational results rather well. A close look at Fig. 4c reveals that the model underestimated the aerosol extinction coefficients of the anthropogenic pollutant event on 22 March but slightly overestimated the extinction coefficients associated with particles having larger total volume depolarization ratios on 30 and 31 March (i.e., dust-dominant case).

#### 4.2 Comparison of aerosol optical depths

Figure 5 shows temporal variations of the aerosol optical depths (AOD) measured by Mie lidar at 532 nm and sky radiometer at 500 nm (Kobayashi et al., 2006, Uchino et al., 2012a) and simulated at 550 nm by MASINGAR-mk2 from 20 to 31 March. To estimate AODs from the lidar data, the extinction coefficient at 225 m was extrapolated to the ground, the extinction coefficient from 15 to 35 km was observed at night on the same day, and  $S$  was assumed to be 50 sr for all altitudes. When clouds and thick aerosols

were present, AODs were not obtained. The sky radiometer was positioned on the roof of the building, which is four stories high and located to the west of the container (brown building in Fig. 1). Although it must be noted that the measured and simulated wavelengths differed slightly, the AODs were almost the same, except for the high aerosol and ozone event on 22 March. The mean bias and the standard deviation of AOD between Mie lidar and sky radiometer was  $0.029 \pm 0.051$ , and that between MASINGAR mk-2 and sky radiometer was  $-0.07 \pm 0.24$  for 20–31 March, except for 12:00–14:00 JST on 22 March. The maximum values of the AODs were 2.1 at 12:00 JST by lidar, 1.92 at 13:00 JST by sky radiometer, and 0.53 at 13:00 JST by MASINGAR-mk2. One possible reason for the large difference in AOD ( $\sim 0.2$ ) between Mie lidar and Sky radiometer data is that we set the reference altitudes 8.2 km and 2.8 km at 12:00 and 13:00 JST on 22 March respectively for the lidar because the backscattered signals were strongly attenuated by the dense aerosol layers below 2 km. This might cause error in AODs for the Mie lidar data. The sky radiometer could have different sight than the Mie lidar. This might be also a possible reason for the difference.

The model underestimated the AODs by factors of about 3.6–4 compared to the sky radiometer and lidar observations. One plausible reason for that is that the model resolution (about 60 km) was insufficient to reproduce the observed prominent peak in which the observed AOD increased from 1.0 to 2.0 in 6 hours. The other plausible reason for the underestimation is the uncertainty of the emissions inventories of aerosol precursors. Grainer et al. (2011) collected various emission inventories and compared them in global scales. They found that differences in Chinese sulfur dioxide ( $\text{SO}_2$ ) emissions in 2000 reached 66% between the lowest and highest emissions and concluded that there was no consensus among the different inventories for the emissions of Chinese  $\text{SO}_2$ . This large variation among the inventories indicates that estimate of  $\text{SO}_2$  emission in China has large error. In their comparison, the MACCity emission which was used in MASINGAR-mk2 simulation, showed the lower amount of Chinese  $\text{SO}_2$  emission among the inventories. This might be responsible for the underestimation of pollution aerosol (sulfate) concentrations. In MASINGAR-mk2, dust emission flux is estimated by a parameterized dust emission scheme and has strong dependency upon various parameters (i.e., soil texture, soil wetness, land use, snow cover fraction, vegetation cover, surface wind speed, etc.). The dust model intercomparison project (DMIP; Uno et al., 2006) reported that simulated dust emission amounts over East Asia among eight dust models (including the former version of MASINGAR) differed sometimes by a factor of ten. These facts indicate that estimate of dust emission also causes large errors. To solve this problem, for example, it might be better to use the near real-time satellite data of  $\text{SO}_2$  and nitrogen dioxide ( $\text{NO}_2$ ) provided by the Ozone Monitoring Instrument (OMI) onboard NASA's Aura satellite (Krotkov et al., 2016), and/or to use a data assimilation technique that integrates model simulation and observation data (Yumimoto et al., 2016).

## 5 Discussion: origin and transport pathways of ozone and aerosol plumes



Figure 7 shows the time-altitude cross sections of total aerosol extinction coefficients at 550 nm, and the ratios of dust extinction coefficients to total aerosol extinction coefficients simulated by MASINGAR-mk2 with potential temperatures over Saga for 20–31 March 2015. For the event on 22 March, the model predicted the dust particles (about 60–100%) in the altitude range 1–3 km, and sulfate (about 40–60%) and dust (about 30–40%) particles below 1 km. The number of the parenthesis represents the ratio of each component's extinction coefficient to the total extinction coefficient. The dust particles descended to the surface in the afternoon (Fig.7b). For the event on 30 March, MASINGAR mk-2 predicted the dust particles (about 50–100%) for 1–6 km, and sulfate (about 50–80%) and dust (about 0–20%) particles below 1 km in the morning. Mie lidar data support the model prediction because  $D_p$  is high ( $17 \pm 6\%$ ) for 1–3 km and low ( $10 \pm 3\%$ ) below 1 km. For both events, small amounts of organic carbon, black carbon and sea salt particles were predicted.

To identify the origin of the aerosols and related transport processes, three-dimensional backward trajectories of air parcels were calculated with the NOAA Hybrid Single Particle Lagrangian Integrated Trajectory (HYSPRIT) model (Draxler and Hess, 1998; Stein et al., 2015). An air parcel was initially left at altitudes of 1500 m (Fig. 8a) and 500 m (Fig.9a) over the lidar site at Saga. The trajectories were calculated for three days from 21:00 UTC on 21 (06:00 JST on 22) March 2015. Figures 8b and 9b show the time-altitude cross sections of dust and sulfate extinction coefficients simulated by MASINGAR mk-2 along the trajectory paths of Figs. 8a and 9a, respectively. Based on the results of the backward trajectories and the model simulations, the dust and sulfate particles on 22 March could have been transported within about two days from the Gobi Desert and the North China Plain (NCP), respectively, to the measurement site. The MASINGAR mk-2 simulation suggested that the dust particles emitted during 18:00-24:00 UTC on 19 March around 40°N and 130.29°E were responsible for the dust storm captured by the Mie lidar observation. The highest concentrations of SO<sub>2</sub> and NO<sub>2</sub> in the world were observed in NCP for 2013–2015 by the Ozone Monitoring Instrument (OMI) onboard NASA's Aura satellite, as shown in Fig.5 by Krotkov et al. (2016). These gases are important precursors of sulfate particles and ozone. Figure 10 represents the horizontal maps of ozone volume mixing ratios at 925 hPa (about 760 m altitude) simulated by MRI-CCM2 at 21:00 JST on 19, 20, 21 March and at 03:00 JST on 22 March 2015. These maps indicate that the high ozone could be transported from NCP to the Yellow Sea and then Saga within about two days.

Because it was difficult to obtain observational data of surface ozone and sulfate particles in NCP including Beijing on 19-20 March, we refer to the following papers related to those data. According to the ozonesonde measurements made by Wang et al. (2012), ozone concentrations  $\geq 90$  ppbv were observed over Beijing, China in late March. Ma et al. (2016) reported a significant increase of surface ozone from 2003 to 2015 at Shangdianzi (40.65°N, 117.10°E), which is located about 100 km northeast of suburban Beijing, and the maximum daily average 8-h concentrations of ozone appear to have been  $>100$  ppbv in March 2015 based on Fig. 2 in their paper. High PM<sub>2.5</sub> and submicron aerosol concentrations have been observed in Beijing (Zhang et al., 2013; Sun et al., 2015). Ozone and aerosol concentrations may therefore have been high in March 2015 over NCP.

To investigate the vertical transport processes of the aerosol and ozone in the lower troposphere over the measurement site, we show in Fig. 11 the time variations of the top altitudes of the ~~mixed atmospheric boundary layers~~ ~~from two hours after sunrise to two hours before sunset during~~ ~~from 11:10 JST on 20 March through to 14:33 JST on 31 March 2015~~ which were estimated from the 1064 nm range-corrected backscatter signals with a range resolution of 15 m using the wavelet covariance transform method (Baars et al., 2008; Izumi et al., 2016), and those obtained from the radiosonde data at Fukuoka and the JMA Meso-scale Analysis (MA) data over Saga using the parcel method (Holzworth, 1964). When the mixed layers developed in the afternoon, the tops of the mixed layers (1.5–2 km) estimated by Mie lidar were almost consistent with those by MA. ~~However, Mie lidar had a tendency to detect the residual layers in the night and morning time, e.g., 21–22 March.~~ Although the radiosonde data at 9:00 JST on 22 March found the top of the mixed layer was 117 m (Stull, 1988), it was difficult for Mie lidar to detect the mixed layer because the lowest altitude of the Mie lidar measurement was 225 m.

The dust particles originated from the Gobi Desert arrived at 1–3 km altitudes ~~above the residual layer~~ over the lidar site at 06:00 JST on 22 March. When the mixed layer developed to 1.5–2 km at 11:00–15:00 JST on 22, the dust particles were supposed to be mixed into the boundary layer and then reached the surface by the entrainment, as simulated in Fig.7b. This could result in the sharp increase in PM<sub>2.5</sub> concentrations at the surface after 11:00 JST, as shown in Fig.4. The similar phenomenon was observed over the northern Kyushu area during the dust event in late May–early June 2014 (Uno et al., 2016). A similar high-surface-ozone event was observed by eight ozonesonde measurements during 6–9 June 2003 over the Seoul metropolitan region (Oh et al., 2010).

## 6. Concluding remarks

By using ozone DIAL and a two-wavelength polarization (Mie) lidar, we made continuous measurements of ozone and aerosol concentrations over Saga during 20–31 March 2015. High ozone and high aerosol concentrations that occurred nearly simultaneously were observed in the altitude range 0.5–1.5 km from 03:00 to 20:00 JST on 22 March 2015. The ozone volume mixing ratio was larger than 100 ppbv. The aerosol extinction coefficient and AOD at 532 nm were larger than 0.5 km<sup>-1</sup> and 1.5, respectively.

Backward trajectory analysis and the simulations by the MASINGAR mk-2 and the MRI-CCM2 models indicated that the mineral dust particles originated from the Gobi Desert and an air mass with high ozone and aerosol (mainly sulfate) concentrations originated from the North China Plain could have been transported over the lidar site within about two days. Based on the lidar and surface measurement data and the simulation by MASINGAR-mk2, there is a possibility that the air mass with high ozone and aerosol concentrations could have been transported from the lower troposphere to the surface by vertical mixing when the planetary boundary layer developed in the afternoon of 22 March 2015. The combination of ozone DIAL measurements with surface in-situ ozone measurements is very useful for studying the process of descent of high ozone concentrations in the lower troposphere to the surface and

the impacts on surface air quality. Such measurements of pollution plumes that descend from the free troposphere to the surface are highly recommended (HTAP, 2010).

The MRI-CCM2 could approximately reproduce the high-ozone volume-mixing ratios after some modifications of physical and chemical parameters. MASINGAR mk-2 successfully predicted high aerosol concentration events, but the predicted peak AOD was about one-third of the observed AOD. For further improvement of these models, it will be important to continue comparing these models with ozone DIAL, Mie lidar, and surface in-situ ozone and particle measurements.

*Acknowledgements.* We used radiosonde data measured by the Japan Meteorological Agency and hourly concentrations of surface oxidant and PM<sub>2.5</sub> measured by the Saga Prefectural Environmental Research Center. The NOAA Hybrid Single Particle Lagrangian Integrated Trajectory (HYSPRIT) model was used to calculate backward trajectories of air parcels.

## References

- Akimoto, H., Mukai, H., Nishikawa, M., Murano, K., Hatakeyama, S., Liu, C. M., Buhr, M., Hsu, K. J., Jaffe, D. A., Zhang, L., Honrath, R., Merrill, J. T., and Newell, R. E.: Long-range transport of ozone in the East Asian Pacific rim region, *J. Geophys. Res.*, 101, D1, 1999-2010, 1996.
- Ancellet, G. and Ravetta, F.: Analysis and validation of ozone variability observed by lidar during the ESCOMPTE-2001 campaign, *Atmos. Res.*, 74, 435-459, 2005.
- Anderson, T. L., Masonis, S. J., Covert, D. S., Ahlquist, N. C., Howell, S. G., Clarke, A. D., and McNaughton, C. S.: Variability of aerosol optical properties derived from in situ aircraft measurements during ACE-Asia, *J. Geophys. Res.*, 108, D23, 8647, doi:10.1029/2002JD003247, 2003.
- Baars, H., Ansmann, A., Engelmann, R., and Althausen, D.: Continuous monitoring of the boundary-layer top with lidar, *Atmos. Chem. Phys.*, 8, 7281-7296, 2008.
- Bak, J., Kim, J. H., Liu, X., Chance, K., and Kim, J.: Evaluation of ozone profile and tropospheric ozone retrievals from GEMS and OMI spectra, *Atmos. Meas. Tech.*, 6, 239-249, doi:10.5194/amt-6-239-2013, 2013.
- Banta, R. M., Senff, C. J., White, A. B., Trainer, M., McNider, R. T., Valente, R. J., Mayor, S. D., Alvarez, R. J., Hardesty, R. M., Parrish, D., and Fesenfeld, F. C.: Daytime buildup and nighttime transport of urban ozone in the boundary layer during a stagnation episode, *J. Geophys. Res.*, 103, D17, 22519-22544, 1998.
- Carslaw, D. C.: Evidence of an increasing NO<sub>2</sub>/NO<sub>x</sub> emissions ratio from road traffic emissions, *Atmos. Env.*, 39, 4793-4802, 2005.
- Cattrall, C., Reagan, J., Thome, K., and Dubovik, O.: Variability of aerosol and spectral lidar and backscatter and extinction ratios of key aerosol types derived from selected Aerosol Robotic Network locations, *J. Geophys. Res.*, 110, D10S11, doi:10.1029/2004JD005124, 2005.
- Deushi, M. and Shibata, K.: Development of a Meteorological Research Institute Chemistry-Climate Model version 2 for the study of tropospheric and stratospheric chemistry, *Pap. Meteorol. Geophys.*, 62, 1-46, doi:10.2467/mripapers.62.1, 2011.
- Draxler, R. R. and Hess, G. D.: An overview of the HYSPLIT\_4 modeling system for trajectories, dispersion, and deposition, *Aust. Meteor. Mag.*, 47, 295-308, 1998.
- Eisele, H. and Trickl, T.: Improvements of the aerosol algorithm in ozone lidar data processing by use of evolutionary strategies, 44, 2638-2651, 2005.
- Fernald, F. G.: Analysis of atmospheric lidar observations: some comments, *Appl. Opt.*, 23, 652-653, 1984.
- Granier, C., Bessagnet, B., Bond, T., D'Angiola, A., van der Gon, H. D., Frost, G. J., Heil, A., Kaiser, J. W., Kinne, S., Klimont, Z., Kloster, S., Lamarque, J. -F., Liousse, C., Masui, T., Meleux, F., Mievville, A., Ohara, T., Raut, J.-C., Riahi, K., Schultz, M. G., Smith, S. J., Thompson, A., van Aardenne, J., van der Werf, G. R., and van Vuuren, D. P.: Evolution of anthropogenic and biomass burning emission of air pollutants at global and regional scales during the 1980–2010 period, *Clim. Change*, 109, 163–190, 2011.

Hara, Y., Yumimoto, K., Uno, I., Shimizu, A., Sugimoto, N., Liu, Z., and Winker, D. M.: Asian dust outflow in the PBL and free atmosphere retrieved by NASA CALIPSO and an assimilated dust transport model, *Atmos. Chem. Phys.*, 9, 1227-1239, 2009.

Hemispheric Transport of Air Pollution (HTAP) 2010, Part A: Ozone and particulate matter, edited by: Dentener, F., Keating, T., and Akimoto, H., Air Pollution Studies No. 17, United Nations, New York and Geneva, 278 pp., 2010.

Holzworth, G. C.: Estimates of mean maximum mixing depths in the contiguous United States, *Mon. Weather Rev.*, 92, 235-242, 1964.

Houweling, S., Hartmann, W., Aben, I., Schrijver, H., Skidmore, J., Roelofs, G.-J., and Breon, F.-M.: Evidence of systematic errors in SCIAMACHY-observed CO<sub>2</sub> due to aerosols, *Atmos. Chem. Phys.*, 5, 3003-3013, 2005.

Intergovernmental Panel on Climate Change (IPCC): Climate Change 2013: The Physical Science Basis: Contribution of Working Group I to the Fifth Assessment Report of the Intergovernmental Panel on Climate Change, edited by: Stocker, T.F., Qin, D., Plattner, G.-K., Tignor, M., Allen, S.K., Boschung, J., Nauels, A., Xia, Y., Bex, V., and Midgley, P.M., Cambridge University Press, Cambridge, United Kingdom and New York, NY, USA, 1535 pp, doi:10.1017/CBO9781107415324, 2013.

Iwasaka, Y., Yamato, M., Imasu, R., and Ono, A.: Transport of Asian dust (KOSA) particles; importance of weak KOSA events on the geochemical cycle of soil particles, *Tellus*, 40B, 494-503, 1988:

Izumi, T., Uchino, O., Sakai, T., Nagai, T., and Morino, I.: Mixed layer height calculated from Mie lidar data, submitted to Tenki, 2016 (in Japanese).

Kobayashi, E., Uchiyama, A., Yamazaki, A., and Matsuse, K: Application of the maximum likelihood method to the inversion algorithm for analyzing aerosol optical properties from sun and sky radiance measurements, *J. Meteor. Soc. Jpn.*, 84, 1047-1062, 2006.

Kourtidis, K., Zerefos, C., Rapsomanikis, S., Simeonov, V., Balis, D., Perros, P. E., Thompson, A. M., Witte, J., Calpini, B., Sharobiem, W. M., Papayannis, A., Mihalopoulos, N., and Drakou, R.: Regional levels of ozone in the troposphere over eastern Mediterranean, *J. Geophys. Res.*, 107, D18, 8140, doi:10.1029/2000JD000140, 2002.

Krotkov, N. A., McLinden, C. A., Li, C., Lamsal, L. N., Celarier, E. A., Marchenko, S. V., Swartz, W. H., Bucsela, E. J., Joiner, J., Duncan, B. N., Boersma, K. F., Veefkind, J. P., Levelt, P. F., Fioletov, V. E., Dickerson, R. R., He, H., Lu, Z., and Streets, D. G.: Aura OMI observations of regional SO<sub>2</sub> and NO<sub>2</sub> pollution changes from 2005 to 2015, *Atmos. Chem. Phys.*, 16, 4605-4629, doi:10.5194/acp-16-4605-2016, 2016.

Kuang, S., Newchurch, M. J., Burris, J., Wang, L., Buckley, P. I., Johnson, S., Knupp, K., Huang, G., Phillips, D., and Cantrell, W.: Nocturnal ozone enhancement in the lower troposphere observed lidar, *Atmos. Environ.*, 45, 6078-6084, 2011.

Kurokawa, J., Ohara, T., Morikawa, T., Hanayama, S., Janssens-Maenhout, G., Fukui, T., Kawashima, K., and Akimoto, H.: Emissions of air pollutants and greenhouse gases over Asian regions during 2000–2008: Regional Emission inventory in ASia (REAS) version 2, *Atmos. Chem. Phys.*, 13, 11019–

11058, doi: 10.5194/acp-13-11019-2013, 2013.

Ma, Z., Xu, J., Quan, W., Zhang, Z., Lin, W., and Xu, X.: Significant increase of surface ozone at a rural site, north of eastern China, *Atmos. Chem. Phys.*, 16, 3969-3977, doi:10.5194/acp-16-3969-2016, 2016.

Murayama, T., Sugimoto, N., Uno, I., Kinoshita, K., Aoki, K., Hagiwara, N., Liu, Z., Matsui, I., Sakai, T., Shibata, T., Arao, K., Sohn, B. J., Won, J. G., Yoon, S. C., Li, T., Zhou, J., Hu, H., Abo, M., Iokibe, K., Koga, R., and Iwasaka, Y.: Ground-based network observation of Asian dust events of April 1998 in east Asia, *J. Geophys. Res.*, 106, D16, 18345-18359, 2001.

Nakazato, M., Nagai, T., Sakai, T., and Hirose, Y.: Tropospheric ozone differential-absorption lidar using stimulated Raman scattering in carbon dioxide, *Appl. Opt.*, 46, 2269-2279, 2007.

Oh, I.-B., Kim, Y.-K., Hwang, M.-K., Kim, C.-H., Kim, S., and Song, S.-K.: Elevated ozone layers over the Seoul metropolitan region in Korea: evidence for long-range ozone transport from eastern China and its contribution to surface concentrations, *J. Appl. Meteor. and Climat.*, 49, 203-220, doi:10.1175/2009JAMC2213.1, 2010.

Ohara, T., Akimoto, H., Kurokawa, J., Horii, N., Yamaji, K., Yan, X., and Hayasaka, T.: An Asian emission inventory of anthropogenic emission sources for the period 1980-2020, *Atmos. Chem. Phys.*, 7, 4419-4444, doi:10.5194/acp-7-4419-2007, 2007.

Ohyama, H., Kawakami, S., Shiomi, K., and Miyagawa, K.: Retrievals of total and tropospheric ozone from GOSAT thermal infrared spectral radiances, *IEEE Trans. Geosci. Remote Sens.*, 50, 1770-1784, doi:10.1109/TGRS.2001.2170178, 2012.

Sakai, T., Nagai, T., Nakazato, M., Mano, Y., and Matsumura, T.: Ice clouds and Asian dust studied with lidar measurements of particle extinction-to-backscatter ratio, particle depolarization, and water-vapor mixing ratio over Tsukuba, *Appl. Opt.*, 42, 7103-7116, 2003.

Stein, A. F., Draxler, R. R., Rolph, G. D., Stunder, B. J. B., Cohen, M. D., and Ngan, F.: NOAA's HYSPLIT atmospheric transport and dispersion modeling system, *Bull. Amer. Meteor. Soc.*, 96, 2059-2077, 2015.

Stull, R. B.: An introduction to boundary layer meteorology, Klumer Academic Publications, 670 pp, 1988.

Sun, Y. L., Wang, Z. F., Du, W., Zhang, Q., Wang, Q. Q., Fu, P. Q., Pan, X. L., Li, J., Jayne, J., and Worsnop, D. R.: Long-term real-time measurements of aerosol particle composition in Beijing, China: seasonal variations, meteorological effects, and source analysis, *Atmos. Chem. Phys.*, 15, 10149-10165, doi:10.5194/acp-15-10149-2015, 2015.

Tanaka, T. Y., Orito, K., T. T. Sekiyama, Shibata, K., Chiba, M., and Tanaka, H.: MASINGAR, a global tropospheric aerosol chemical transport model coupled with MRI/JMA98 GCM: Model description, *Pap. Meteor. Geophys.*, 53(4), 119-138, 2003.

Uchino, O. and Tabata, I.: Mobile lidar for simultaneous measurements of ozone, aerosols, and temperature in the stratosphere, *Appl. Opt.*, 30, 2005-2012, 1991.

Uchino, O., Kikuchi, N., Sakai, T., Morino, I., Yoshida Y., Nagai, T., Shimizu, A., Shibata, T.,

- Yamazaki, A., Uchiyama, A., Kikuchi, N., Oshchepkov, S., Brill, A., and Yokota, T., Influence of aerosols and thin cirrus clouds on the GOSAT-observed CO<sub>2</sub>: a case study over Tsukuba, *Atmos. Chem. Phys.*, 12, 3393–3404, doi:10.5194/acp-12-3393-2012, 2012a.
- Uchino, O., Sakai, T., Nagai, T., Nakamae, K., Morino, I., Arai, K., Okumura, H., Takubo, S., Kawasaki, T., Mano, Y., Matsunaga, T., and Yokota, T., On recent (2008–2012) stratospheric aerosols observed by lidar over Japan, *Atmos. Chem. Phys.*, 12, 11975–11984, doi:10.5194/acp-12-11975-2012, 2012b.
- Uchino, O., Sakai, T., Nagai, T., Morino, I., Maki, T., Deushi, M., Shibata, K., Kajino, M., Kawasaki, T., Akaho, T., Takubo, S., Okumura, H., Arai, K., Nakazato, M., Matsunaga, T., Yokota, T., Kawakami, S., Kita, K., and Sasano, Y.: DIAL measurement of lower tropospheric ozone over Saga (33.24°N, 130.29°E), Japan, and comparison with a chemistry–climate model, *Atmos. Meas. Tech.*, 7, 1385–1394, doi:10.5194/amt-7-1385-2014, 2014.
- Uno, I., Wang, Z., Chiba, M., Chun, Y. S., Gong, S. L., Hara, Y., Jung, E., Lee, S.-S., Liu, M., Mikami, M., Music, S., Nickovic, S., Satake, S., Shao, Y., Song, Z., Sugimoto, N., Tanaka, T., and Westphal, D. L.: Dust model intercomparison (DMIP) study over Asia: Overview, *J. Geophys. Res.*, 111, D12213, doi:10.1029/2005JD006575, 2006.
- Uno, I., Pan, X., Itahashi, S., Yumimoto, K., Hara, Y., Kuribayashi, M., Yamamoto, S., Shimohara, T., Tamura, K., Ogata, Y., Osada, K., Kamikuchi, Y., Yamada, S., and Kobayashi, H.: Overview of long-range yellow sand and high concentration of air pollution observed over the northern Kyusyu area in late May-early June 2014, *J. Jpn. Soc. Atmos. Environ.*, 51, 44-57, 2016.
- Veefkind, J. P., Aben, I., McMullan, K., Förster, H., de Vries, J., Otter, G., Claas, J., Eskes, H. J., de Haan, J. F., Kleipool, Q., van Weele, M., Hasekamp, O., Hoogeveen, R., Landgraf, J., Snel, R., Tol, P., Ingmann, P., Voors, R., Kruizinga, B., Vink, R., Visser, H., and Levelt, P. F.: TROPOMI on the ESA Sentinel-5 Precursor: A GMES mission for global observations of the atmospheric composition for climate, air quality and ozone layer applications, *Remote Sens. Environ.*, 120, 70-83, 2012.
- Wang, Y., Konopka, P., Liu, Y., Che, H., Müller, R., Plöger, F., Riese, M., Cai, Z., and Lü, D.: Tropospheric ozone trend over Beijing from 2002-2010: ozonesonde measurements and modeling analysis, *Atmos. Chem. Phys.*, 12, 8389-8399, doi:10.5194/acp-12-8389-2012, 2012.
- Yamaji, K., T. Ohara, T., Uno, I., Tanimoto, H., Kurokawa, J., and Akimoto, H.: Analysis of the seasonal variation of ozone in the boundary layer in East Asia using the Community Multi-scale Air Quality model: What controls surface ozone levels over Japan?, *Atmos. Environ.*, 40, 1856-1868, 2006.
- Yue, X. and Unger, N., Ozone vegetation damage effects on gross primary productivity in the United States, *Atmos. Chem. Phys.*, 14, 9137-9153, doi:10.5194/acp-14-9137-2014, 2014.
- Yukimoto, S., Adachi, Y., Hosaka, M., Sakami, T., Yoshimura, H., Hirabara, M., Tanaka, T. Y., Shindo, E., Tsujino, H., Deushi, M., Mizuta, R., Yabu, S., Obata, A., Nakano, H., Koshiro, T., Ose, T., and Kitoh, A.: A new global climate model of the Meteorological Research Institute: MRI-CGCM3 —Model Description and Basic Performance—, *J. Meteorol. Soc. Jpn.*, 90A, 23-64, doi:10.2151/jmsj.2012-A02, 2012.
- Yumimoto, K., Nagao, T. M., Kikuchi, M., Sekiyama, T. T., Murakami, H., Tanaka, T. Y., Ogi, A., Irie, H.,

Khatari, P., Okumura, H., Arai, K., Morino, I., Uchino, O., and Maki, T.: Aerosol data assimilation using data from Himawari-8, a next-generation geostationary meteorological satellite, *Geophys. Res. Lett.*, 43, doi:10.1002/2016GL069298.

Zhang, R., Jing, J., Tao, J., Hsu, S.-C., Wang, G., Cao, J., Lee, C. S. L., Zhu, L., Chen, Z., Zhao, Y., and Shen, Z.: Chemical characterization and source apportionment of PM<sub>2.5</sub> in Beijing: seasonal perspective, *Atmos. Chem. Phys.*, 13, 7053-7074, doi:10.5194/acp-13-7053-2013, 2013.



**Table 1.** Characteristics of Mie lidar

<hr/>			
Transmitter			
Laser	Nd:YAG		
Wavelength	532 nm		1064 nm
Pulse energy	130 mJ		130 mJ
Pulse repetition rate		10 Hz	
Pulse width		8 ns	
Beam divergence	0.2 mrad		0.2 mrad
<hr/>			
Receiver			
Telescope type	Schmidt Cassegrain		
Telescope diameter	30.5 cm		
Focal length	3048 mm		
Field of view	1 mrad		
Polarization	P and S		None
Number of channels	3		1
Interference filter			
Center wavelength	532.0 nm		1064.1 nm
Bandwidth (FWHM)	0.29 nm		0.38 nm
Transmission	0.66		0.58
Detectors	PMT		APD
	(Hamamatsu R3234-01)		(EG&G C30956EH)
Signal processing	12bit A/D + Photon counting		
Time resolution	1 min		
Vertical resolution	7.5 m		
<hr/>			

**Table 2.** Characteristics of tropospheric ozone DIAL system

<hr/>						
Transmitter						
Pump laser	Nd:YAG					
Wavelength	266 nm					
Pulse energy	107 mJ					
Pulse repetition rate	10 Hz					
Pulse width	8 ns					
Raman active gas	CO <sub>2</sub>					
Stokes lines	276 nm	287 nm	299 nm	312 nm		
Pulse energy	7.5 mJ	9.1 mJ	8.4 mJ	No. meas.		
Beam divergence	0.1 mrad					
<hr/>						
Receiver						
Telescope type	Newtonian			Prime focus (fiber coupled)		
Telescope diameter	49 cm			10 cm		
Focal length	1750 mm			320 mm		
Field of view	1 mrad			3 mrad		
Interference filter						
Center wavelength	287.2 nm	299.0 nm	312.0 nm	276.1 nm	287.2 nm	
Bandwidth (FWHM)	1.02 nm	1.15 nm	0.82 nm	1.07 nm	1.05 nm	
Transmission	0.18	0.32	0.36	0.17	0.21	
Detectors	PMT (Hamamatsu R3235-01)					
Signal processing	12bit A/D + Photon counting					
Time resolution	1 min					
Vertical resolution	7.5 m					



**Figure 1.** Mie lidar and ozone DIAL (right) were installed in the container at the left on the ground (left).

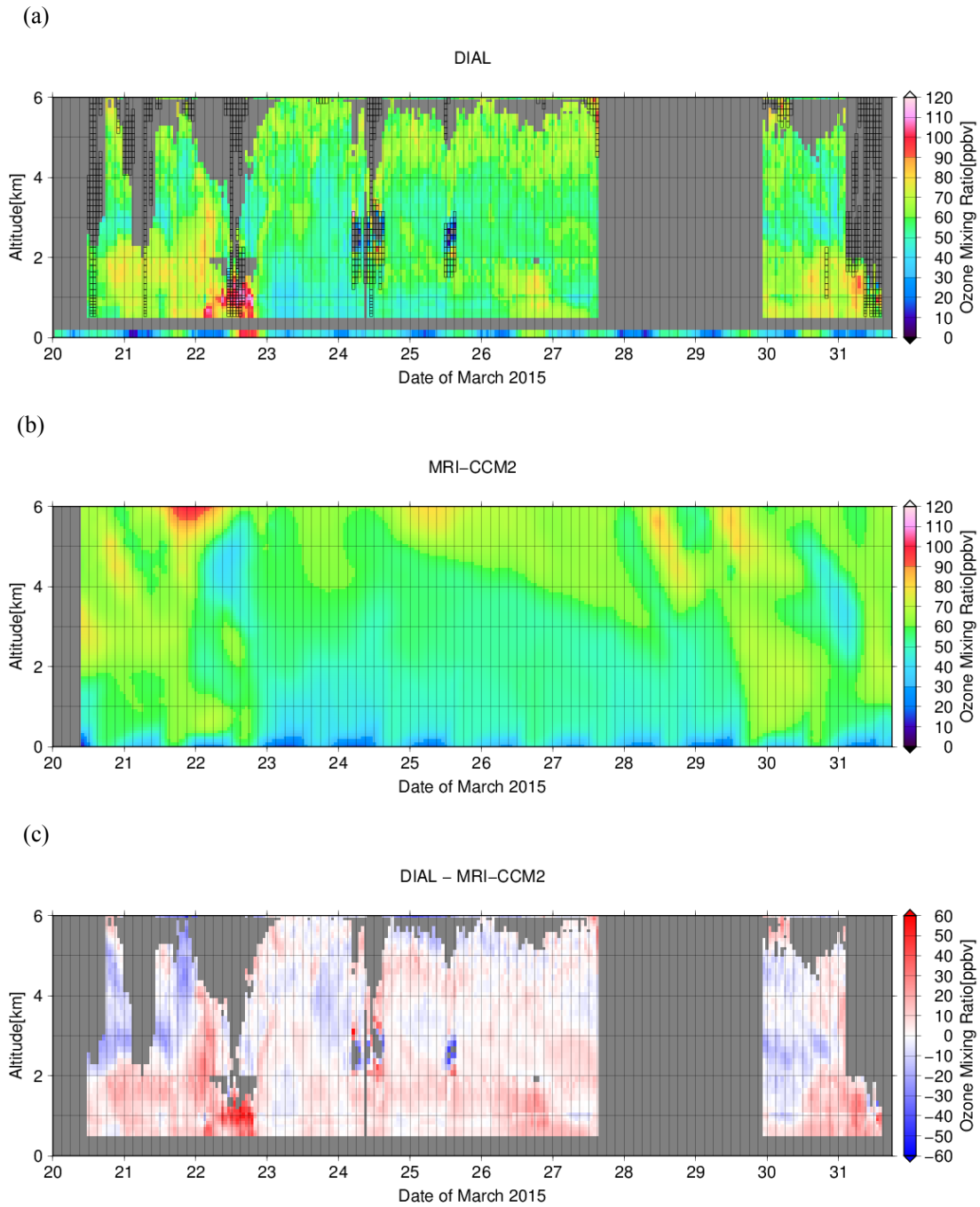


**Figure 2.** Time-altitude cross-sections of (a) ozone volume mixing ratios observed by DIAL over Saga from 11:10 JST on 20 March to 14:33 JST on 31 March 2015, (b) the ratios simulated by a modified MRI-CCM2 for 20–31 March 2015, and (c) the difference between the observed and simulated ozone volume mixing ratios (a–b). Gray regions indicate areas where there were no observational data or the statistical errors were larger than 10%. Regions enclosed with black rectangles are areas where the data were affected by aerosols and/or clouds. The lowest row in Fig. 2a shows photochemical oxidant (ozone) volume mixing ratios at Takagimachi in Saga city as measured by the Saga Prefectural Environmental Research Center.

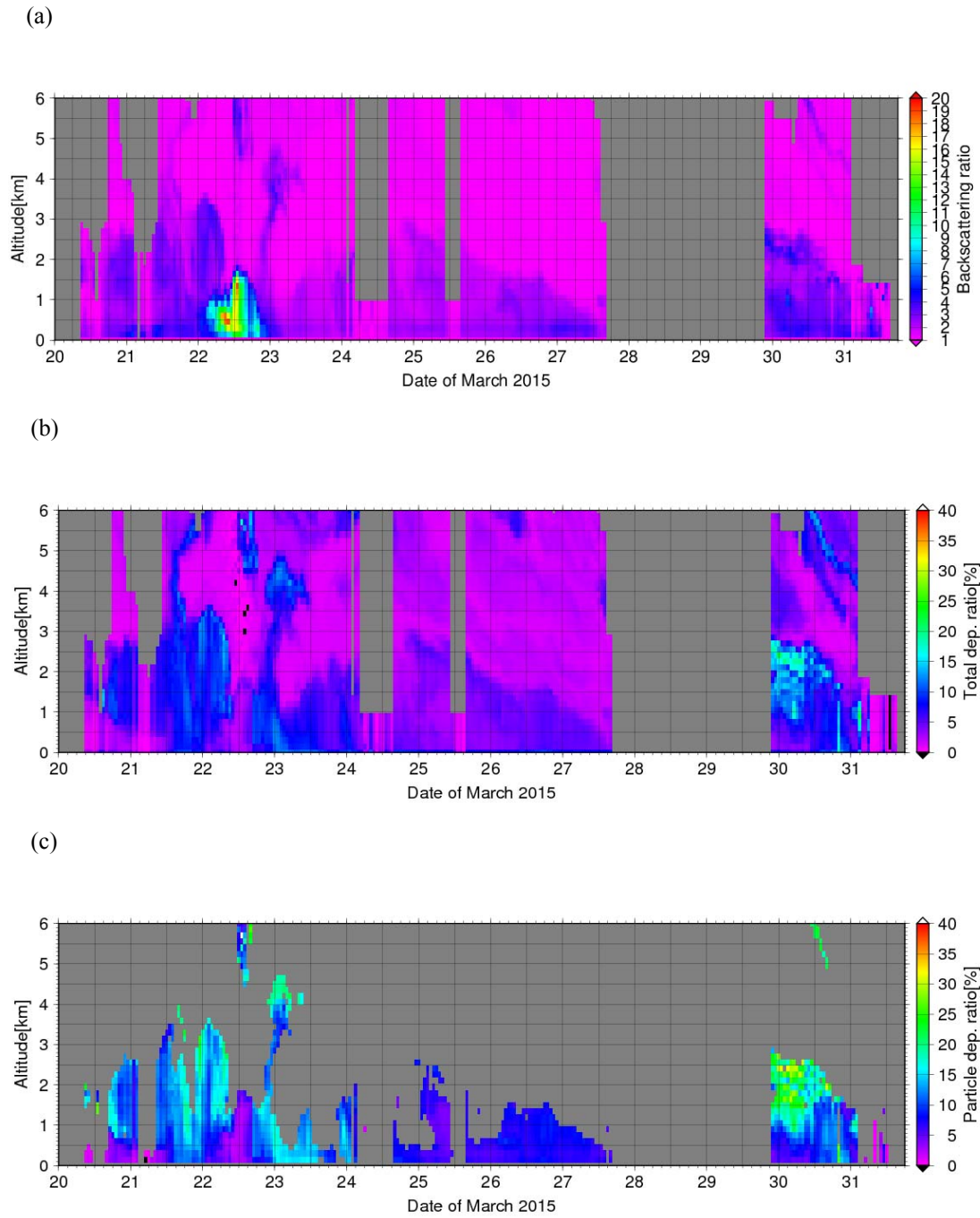


**Figure 3.** Time-altitude cross-sections of (a) backscattering ratios, (b) total volume depolarization ratios, and (c) particle depolarization ratios for  $R$  larger or equal to 2.0 at 532 nm observed by Mie lidar at Saga from 11:10 JST on 20 March to 14:33 JST on 31 March 2015. Lidar observations were not available from 15:56 JST on 27 March to 21:58 JST on 29 March 2015 mainly because of rainy or cloudy conditions. Gray regions are areas where there were no observational data or where the observations were affected by clouds.

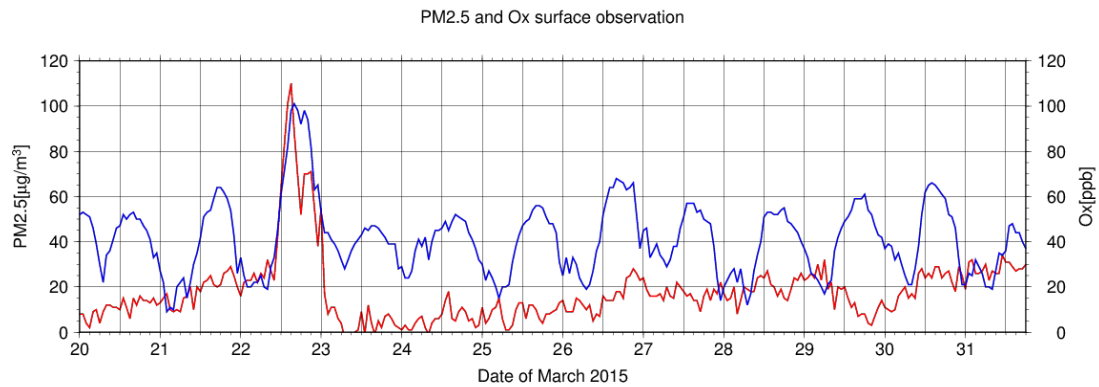


**Figure 4.** Hourly (JST) data of surface PM2.5 (red line) and Ox (blue line) measured by the Saga Prefectural Environmental Research Center for 20-31 March 2015. The volume mixing ratio of Ox was considered to be that of ozone.

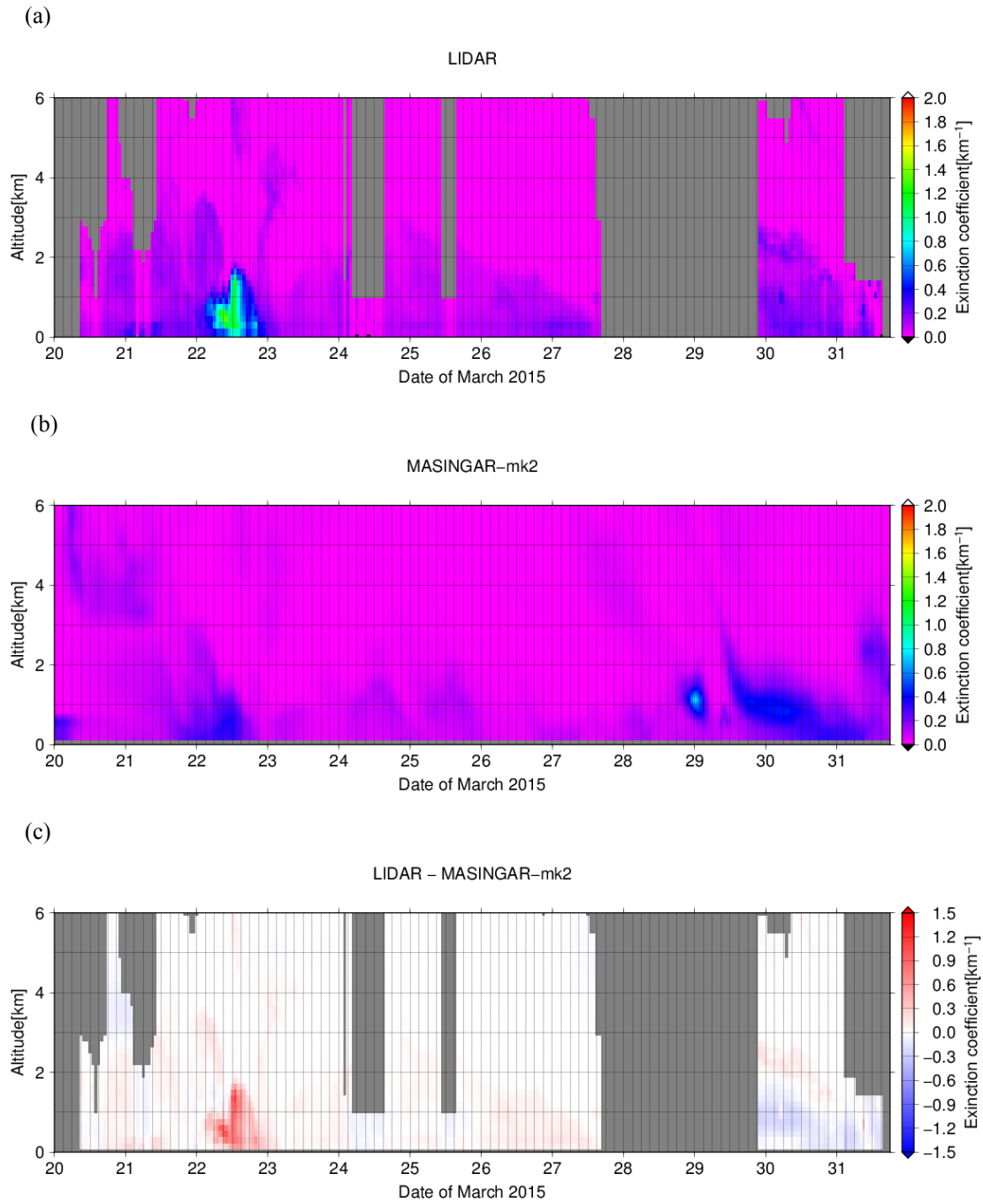


**Figure 5.** Time-altitude cross sections of (a) aerosol extinction coefficients observed by Mie lidar at 532 nm over Saga from 11:10 JST on 20 March to 14:33 JST on 31 March 2015, (b) the coefficients simulated by MASINGAR-mk2 at 550 nm for 20–31 March 2015, and (c) the difference between the Mie lidar observations and the simulation (a–b). Gray regions represent areas where there were no observational data.

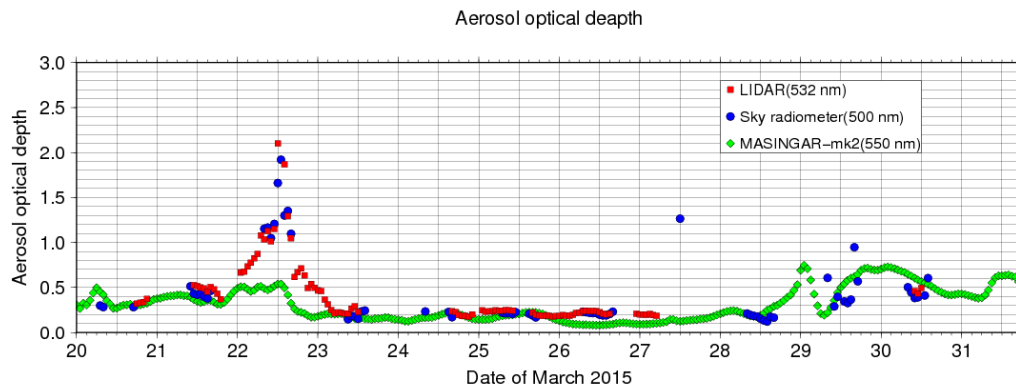
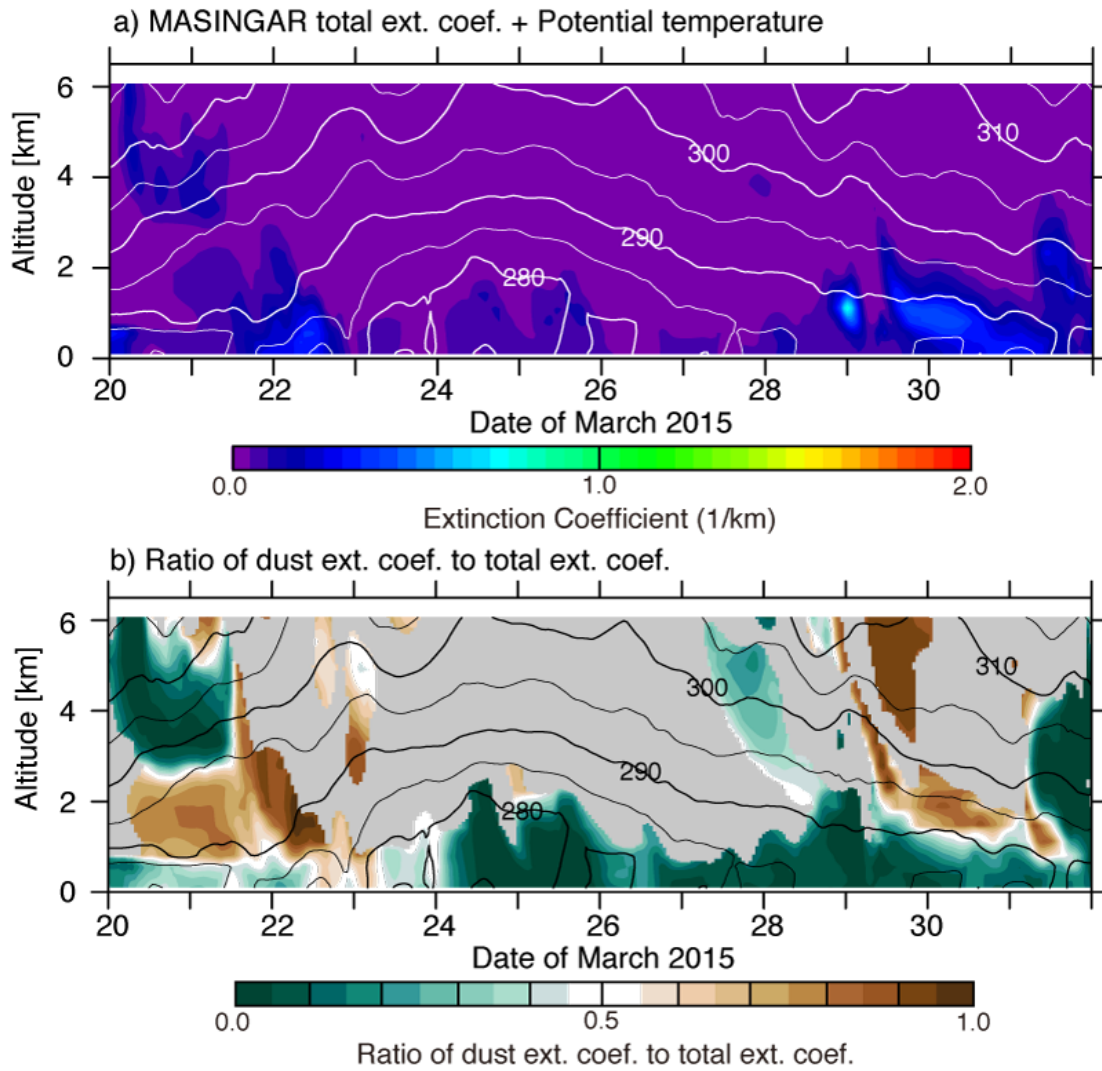


**Figure 6.** Temporal variation of the aerosol optical depth (AOD) measured by Mie lidar at 532 nm (red circles), by sky radiometer at 500 nm (blue circles), and simulated at 550 nm by MASINGAR-mk2 (green circles).



815



816

817

818 **Figure 7.** Time (JST)-altitude cross sections of (a) total aerosol extinction coefficients at 550 nm (color  
819 shading) and (b) ratios of dust extinction coefficient to total aerosol extinction coefficient (color shading)  
820 simulated by MASINGAR-mk2 with potential temperatures (black contours) over Saga for 20-31 March  
821 2015. The gray regions in Fig. 7b indicate that the simulated total aerosol extinction coefficient is less  
822 than 0.02.

823

824

825

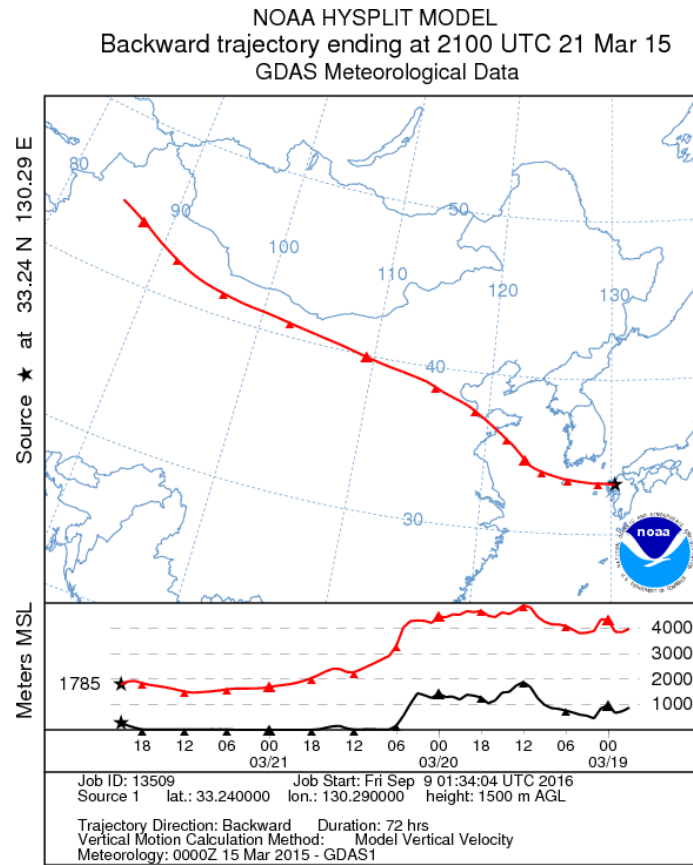
826

827

828

829

(a)



(b)

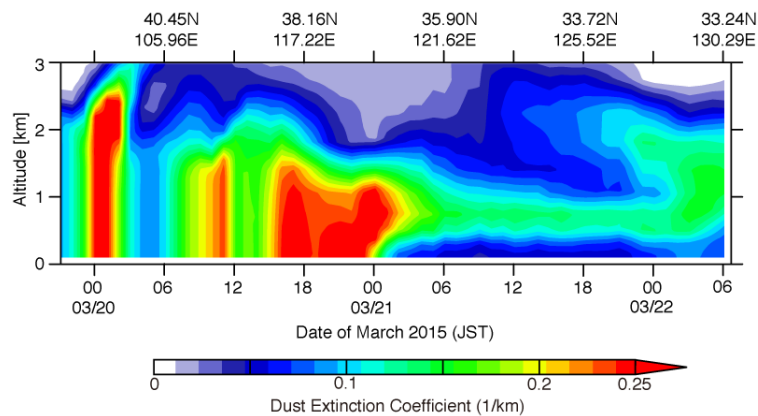
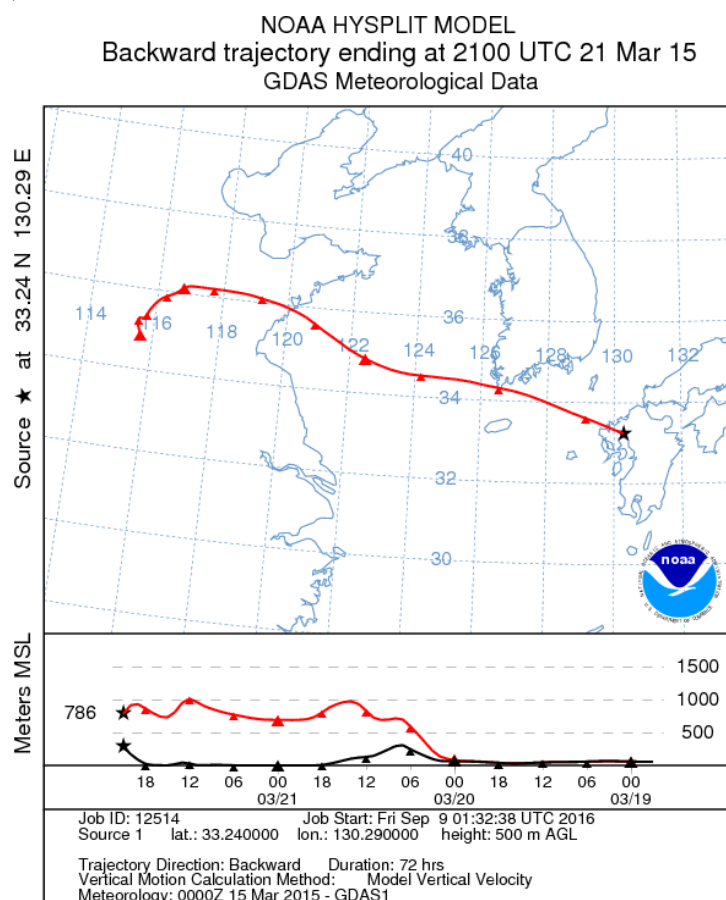


**Figure 8.** (a) 72-h HYSPLIT-model backward trajectory (red line) and terrain height (black line) from Saga at 1500 m above ground level (AGL) ending at 06:00JST on 22 May 2015. (b) Time-altitude cross section of dust extinction coefficient simulated by MASINGAR mk-2 along the trajectory path.

(a)



(b)

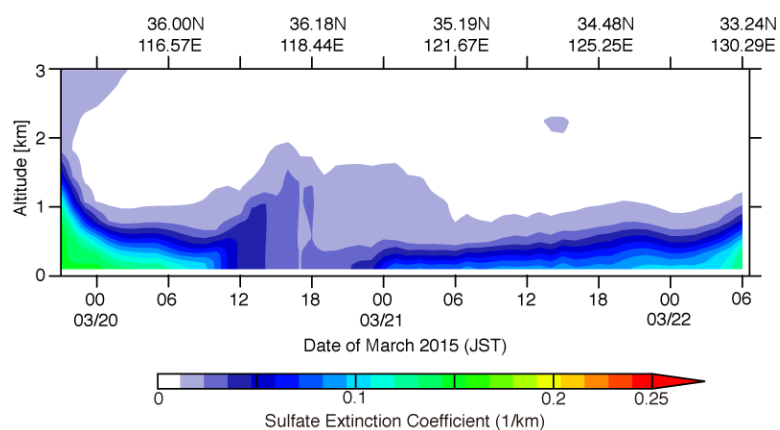


**Figure 9.** Same as Fig. 8 but for 500 m AGL.

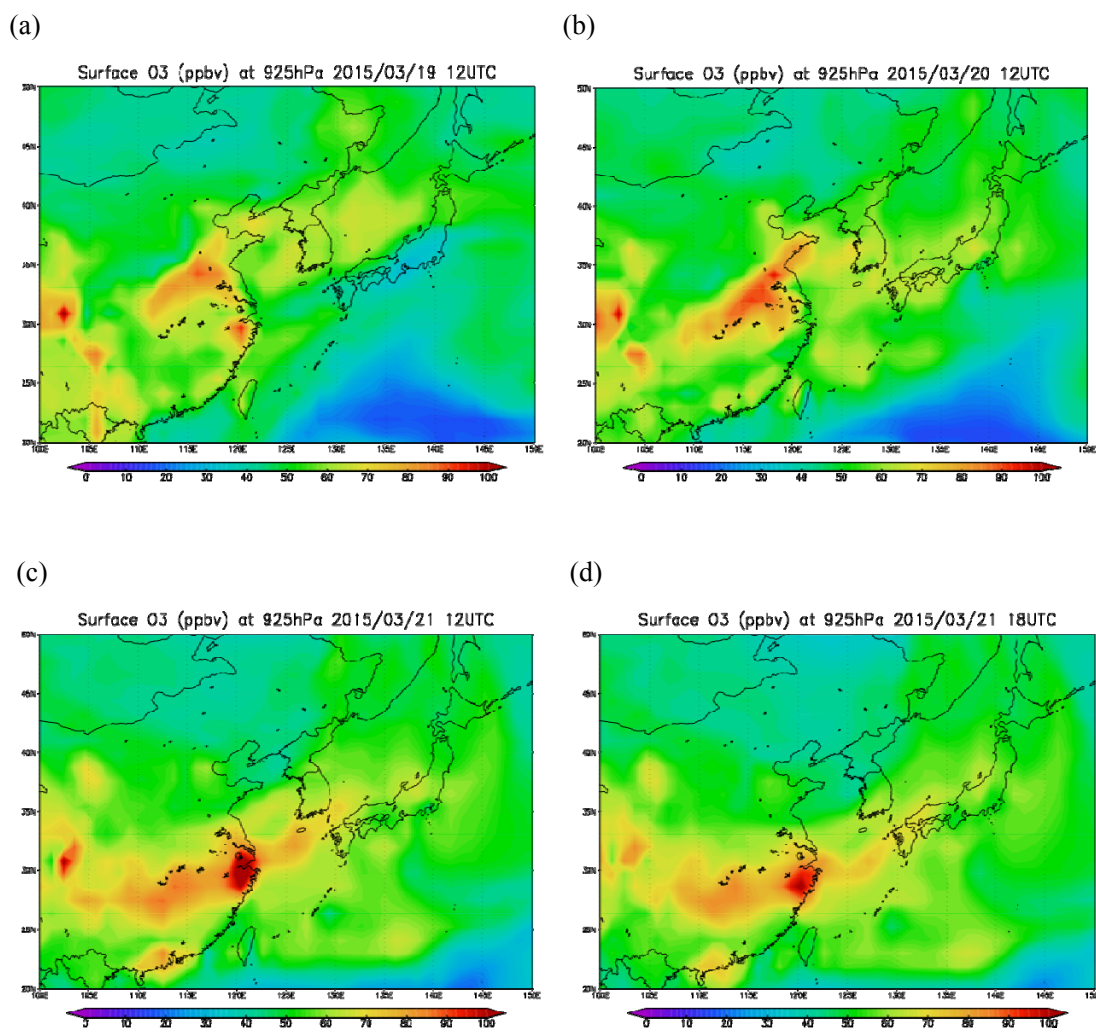
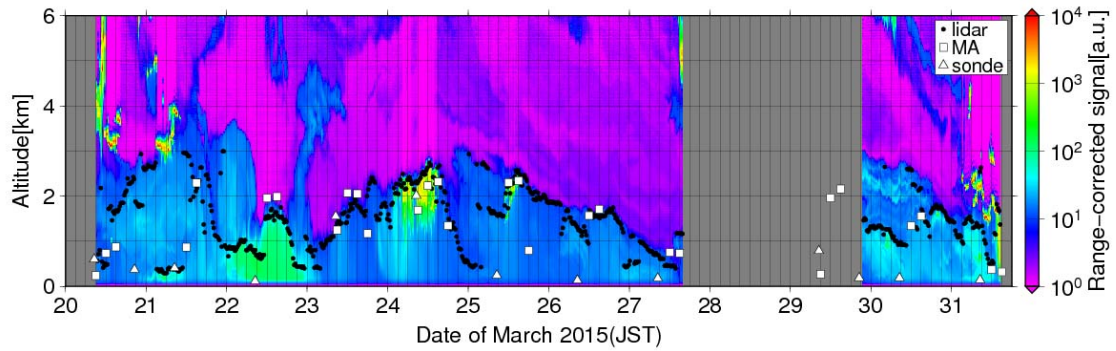


**Figure 10.** Horizontal maps of ozone volume mixing ratios in ppbv predicted by MRI-CCM2 for 925 hPa pressure level (about 760 m altitude) at 21:00 JST (JST=UT+9) on (a) 19, (b) 20, (c) 21 March and (d) 03:00 JST on 22 March 2015.

Old figure (delete)



Revised figure

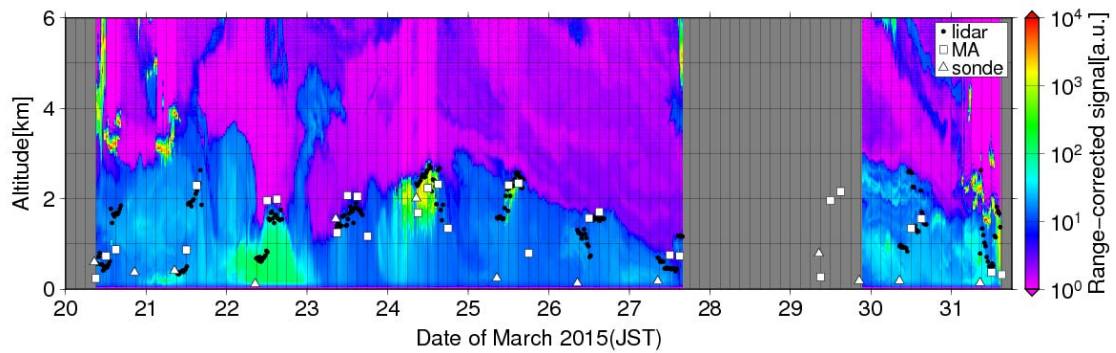


**Figure 11.** Time-altitude cross section of (color shaded) range-corrected backscatter signal at 1064 nm and the tops of the ~~mixed atmospheric boundary~~ layers estimated by Mie lidar (closed black circles), radiosonde (open triangles), and JMA Meso-Scale Meteorological Analysis (open squares) data over Saga from 11:10 JST on 20 March to 14:33 JST on 31 March 2015.

Journal: ACP

Title: Lidar detection of high concentrations of ozone and aerosol transported from Northeast Asia over Saga, Japan

Author(s): Osamu Uchino et al.

MS No.: acp-2016-520

MS Type: Research article

Iteration: Minor Revision

### **Reply to Co-Editor comments and Anonymous Referee #1 comments**

**Co-Editor Decision: Reconsider after minor revisions (Editor review)** (01 Dec 2016) by Yugo Kanaya

Comments to the Author:

Dear Authors,

Thank you for submitting your revised manuscript. Re-evaluation was made by our two reviewers. One suggested accepted as is, and the other requested minor revision. I would appreciate you could further respond to the comments by the reviewer #2. Also, I hope if you could take into account the handling editor's comments below:

The authors wish to thank the Co-Editor and the reviewer #2 for helpful and thoughtful comments. Each comment is addressed individually below. The reference comments are written in black, and our responses are described in red.

1. Although the focus of the manuscript is successfully shifted to the aspect of transport analysis, the Introduction part remained focused on the technical aspects and the authors' works. It is better to add some more general description on O<sub>3</sub> and aerosols pollutions reaching this region in spring from the continent, citing literature (including those not using lidars), touching on what was studied before and what is yet to be analyzed (e.g., three dimensional features of ozone). This will highlight the value of this manuscript.

As suggested, we added the next sentences and 5 references:

Lines 45-50 and line 77 in the revised paper:

The aerosols transported from the East Asia to the western Japan were observed by lidar and their vertical distributions were reported (Iwasaka et al., 1988; Murayama et al., 2001; Hara et al., 2009). On the other hand the ozone pollutions from the Asia were mainly studied by the surface measurements (Akimoto et al., 1996; Yamaji et al., 2006). Continuous ozone vertical distributions by ozone DIAL are very useful for studying the transport process and the origin.

In this paper we report an event during which high concentrations of ozone and aerosols were observed almost simultaneously below an altitude of 1.5 km over Saga on 22 March 2015 by Mie lidar and ozone DIAL, which substantially impacted surface air quality. We also compared the observational results with those simulated by the models.

2. lines 150-151. Is an old-type ozone monitor based on wet chemistry is still under use at this site, where the PAN interference matters?

Ozone monitor is a UV photometer, and we revised as follows:

Lines 159-161:

Because the surface  $O_3$  was observed by an UV photometer, the contribution of other components such as peroxyacetyl nitrate (PAN) to oxidant concentrations was extremely low, and the oxidant volume mixing ratio was considered to be that of ozone.

3. line 181. Add base year of REAS2.1 emission inventory used for modeling.

We added “the REAS 2.1 emission inventory in 2007” in line 188.

4. lines 186 and 194. How is the 20% of systematic error related to the uncertainty of 12% in line 194?

We estimated as follows:

$\text{uncertainty}^2 = (\text{systematic error})^2 + (\text{statistical error})^2$

the uncertainty:  $(0.2^2 + 0.1^2)^{1/2} = 0.22$

the mean value of the uncertainty:  $(0.07^2 + 0.1^2)^{1/2} = 0.12$

5. lines 266-267. The skyradiometer could have different sight than the lidar. This is also a possible reason for the difference.

We added “The sky radiometer could have different sight than the Mie lidar. This might be also a possible reason for the difference.” in lines 276-277.

6. line 296. When the contribution from dust particles is 100%, those from others need to be 0%.

We replaced “(60–100%)”, “(40–60%)”, and “(30–40%)” in lines 306-307 with “(about 60–100%)”, “(about 40–60%)”, and “(about 30–40%)”, respectively, and also corrected line 310 in the same manner.

7. Figure 8(b). There are several regions with increased dust extinction coefficient. Where do the authors think are the source regions of dust? The maximum during 1800 20 March - 0000 21 March is best connected to the increase over Saga; however, the region is over the ocean or the Shandong Peninsula and thus is not likely the source region.

Meteorological fields (e.g., wind velocities and pressure levels) used in the simulation of dust extinction coefficient (i.e., MASINGAR mk-2) are not identical to those used for the backward trajectory (i.e., HYSPLIT). This could explain that there are several regions where dust extinction coefficients are increased. Please find the next figure of dust emission simulated by MASINGAR mk-2 on 19 March (in UTC).



Based on this figure, we added the following sentences in lines 323-325:

The MASINGAR mk-2 simulation suggested that the dust particles emitted during 18:00–24:00 UTC on 19 March around 40°N, 105°E were responsible for the dust storm captured by the Mie lidar observation.

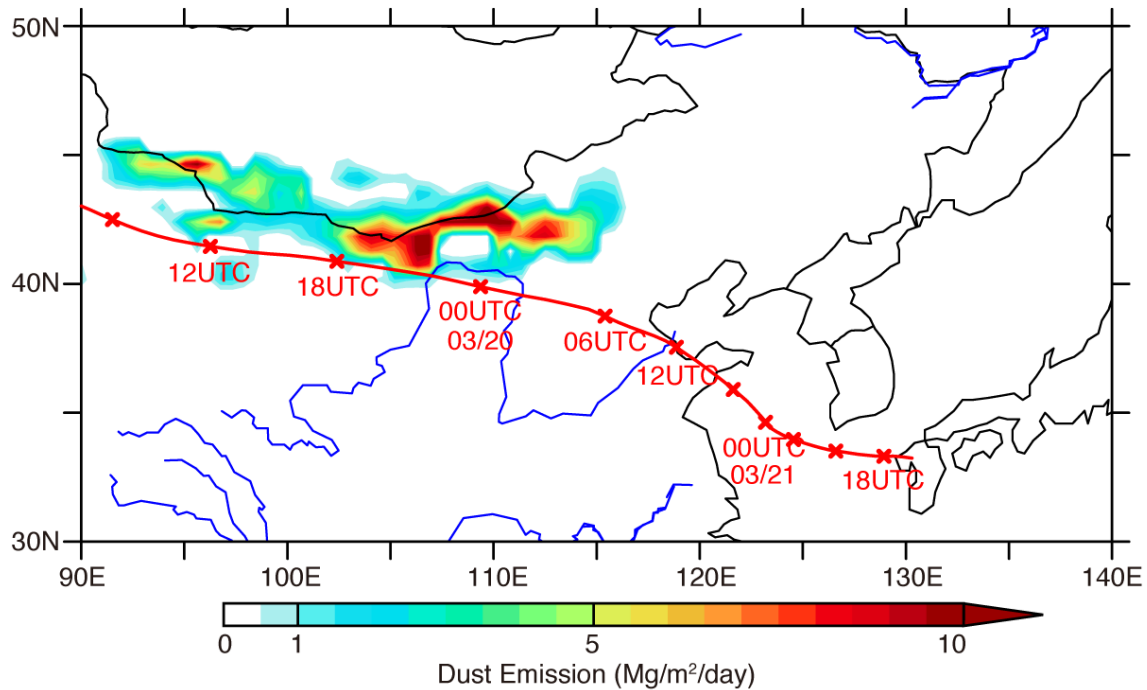


Figure S1, Daily averaged dust emission on 19 March. Red line shows the HYSPLIT-model backward trajectory from Saga at 1500 m above ground level (AGL) ending at 06:00JST on 22 May 2015 (identical to the backward trajectory shown in Figure 8).

**Submitted on 30 Nov 2016**

**Anonymous Referee #2**

In the revised version of the manuscript, a good effort has been done to improve the quality of the paper. Most of the corrections suggested were properly addressed. Before the acceptance of the paper, I recommend to address the following two minor points:

1)The altitudes detected from the lidar measurements (shown in Fig. 11) only in some cases correspond to the atmospheric boundary layer top. For numerous profiles (e.g. from 1200 JST of 20 March to 12 00 JST of 21 March), the method detects altitudes above 2 km that are not realistic boundary layer heights for this season. The algorithm applied to lidar measurements detects vertical gradients of aerosol backscattering, thus the top of aerosol layers that may not be the boundary layer top. A physical identification of the boundary layer top is done by recognizing the temperature inversion from radiosoundings as already



shown in the figure. My recommendation is to screen out all heights detected from lidar data that do not correspond to the boundary layer height shown by the radiosoundings. Also, the difference between residual layer and mixing layer does not seem to be clear in the current paper. Radiosounding can tell the location of both as below the mixing layer the profile of potential temperature is neutral above an unstable layer near the surface and the residual layer corresponds to a neutral profile above a stable layer.

As suggested, Mie lidar had a tendency to detect not realistic mixed layer heights in the nighttime. Therefore we estimated the top altitudes of the mixed layers from two hours after sunrise to two hours before sunset, and revised in lines 342-344 as follows:

“we show in Fig. 11 the time variations of the top altitudes of the ~~mixed atmospheric boundary~~ layers from two hours after sunrise to two hours before sunset during from 11:10 JST on 20 March through to 14:33 JST on 31 March 2015”, and we replaced the old Fig.11 with the revised Fig.11.

And we deleted “However, Mie lidar had a tendency to detect the residual layers in the night and morning time, e.g., 21–22 March.” in lines 349-350 and “ above the residual layer” in line 353.

2) The lidar ratio for both dust and pollution aerosols is the same (50 sr). This is an approximation as shown by the authors themselves: dust seem to have lower lidar ratios than pollution aerosol. I recommend to include in the text of the manuscript the values given in the answers to the reviewers : “Their summaries are as follows: Sakai et al.(2003): Asian dust  $47 \pm 18$  sr, Catrrall et al.(2005): Dust (spheroids)  $42 \pm 4$  sr, SE AsiaPollution  $58 \pm 10$  sr, Anderson et al.(2003): ACE-Asia Pollution (Fine-dominated, submicron portion)  $50 \pm 5$  sr, Dust (Coarse-dominated, Dust-like chemistry, Supermicron portion)  $46 \pm 8$  sr.” and then indicate that as a simplification, they use the same value for both species.

As suggested, the next sentences are added in lines 102-106:

Their summaries are as follows: Sakai et al. (2003): Asian dust  $47 \pm 18$  sr, Catrral et al. (2005): dust (spheroids)  $42 \pm 4$  sr, South East Asia pollution  $58 \pm 10$  sr, Anderson et al. (2003): ACE-Asia pollution (fine-dominated, submicron portion)  $50 \pm 5$  sr, dust (coarse-dominated, dust-like chemistry, supermicron portion)  $46 \pm 8$  sr. As a simplification, we used the same value for both species.